TELKOMNIKA Indonesian Journal of Electrical Engineering
Vol.12, No.2, February 2014, pp. 1236 ~ 1244
DOI: http://dx.doi.org/10.11591/telkomnika.v12i2.3844

Phase Noise Requirement Analysis for Millimeter-Wave Imager Frequency Synthesizer

Jin Zhang*, Zhiping Li, Cheng Zheng, Xianxun Yao, Baohua Yang, Tongfei Yu, Jungang Miao
School of Electronic & Information Engineering, Beihang University (BUAA), Ph./Fax: +86-10-82078330
Beijing, No.37 Xueyuan Road, Haidian District, 100191, P. R. China
*Corresponding author, e-mail: zhangjin850224@139.com

Abstract

In this paper, a nontrivial uncorrelated phase noise analysis is proposed for frequency synthesizer of a passive millimeter-wave Synthetic Aperture Interferometric Radiometer (SAIR) imager named BHU-2D-U designed for concealed weapon detections on human bodies with high imaging rates. This synthesizer provides local oscillators both for millimeter-wave front-ends and intermediate frequency IQ demodulators for the receivers. The influence of synthesizer uncorrelated phase noise in different offset frequency ranges on the visibility phase errors have been systematically investigated with phase noise mismatch requirements drawn. Integrated RMS phase error has been applied to establish uncorrelated phase noise requirements for visibility error control. Measurement results have proved that uncorrelated phase noise does exist among synthesizer output pairs, and the previously defined requirements are achieved with imaging results proposed. In conclusion, the uncorrelated phase noise effects on SAIR visibility errors have been concretized to phase noise design requirements, which have been realized by synthesizer design.

Keywords: *SAIR, frequency synthesizer, uncorrelated phase noise, integrated RMS phase error*

1. Introduction

Various techniques in the area of concealed weapon detection on human bodies have been developed and widely applied for security checks. Compared with active detection systems, such as the X-ray sensors, the passive SAIR (Synthetic Aperture Interferometric Radiometer) imaging system [1] provides several advantages. It only receives rather than emitting high frequency signals and does not result in human health concerns [2]. Moreover, any concealed hazards, including non-metallic weapons and risky powder, can be detected in the obtained image explicitly [3-5].

Though previous SAIR researches have given that coherent FS PN has negligible effects on visibility errors, different receiver channels do produce uncorrelated PN which generates visibility phase errors, a topic which few paper has discussed before. Frequency Synthesizer (FS) provides two local oscillators (LO) for millimeter-wave (mmW) front-ends and IF IQ demodulators, and it is proved that LO uncorrelated phase noise (PN) contributes to these errors. The uncorrelated PN analysis consists of 3 key problems: finding the uncorrelated PN related factors in the phase transfer relations inside the receiver signal chain that cause visibility phase errors; finding the offset frequency range (OFR) whose PN is the major contributor of visibility phase errors and establish proper SAIR FS uncorrelated PN design requirements; realizing FS design with measurements and check if the requirements are reached.

In section 2, the influences of uncorrelated phase noise or phase noise mismatch on visibility phase error are systematically investigated. In section 3 the offset frequency of mmW LO is separated to three OFRs by analysis in section 2, and SAIR uncorrelated PN requirements are proposed. In section 4, the FS design is realized, and the uncorrelated PN requirements are realized with measurements. It is found that uncorrelated PN does exist, and integrated RMS phase error could represent its effects and set limits for its control to limit the visibility phase errors.

Received July 6, 2013; Revised August 26, 2013; Accepted September 19, 2013

2. Phase Noise System-Level Modelling

2.1. System Introduction

A SAIR imager named BHU-2D-U [6] has been developed by Beihang University. It consists of a 48 element U-shape antenna array, and each receiver channel [7-8] is composed of a mmW receiver [9-10] and an IF IQ demodulator. The DSP subsystem computes complex cross-correlations between IF IQ output pairs of all receivers simultaneously, with the results calibrated to form visibility samples, whose IFT generate the brightness temperature of the field of view. Key parameters of BHU-2D-U are summarized in Tab.1, and its simplified block diagram is shown in Figure 1 [6].

Table 1. BHU-2D-U General Specifications

Parameter	Specification (rpm)
Center Frequency	34 GHz
Antenna Array	U-Shape
Field of View	20 deg (Horizontal) 36 deg (Vertical)
Temperature Sensitivity	1~3 K
Effective Distance	2.5~5 m
Range Resolution	6.5 cm @ 3 m
System Bandwidth	200 MHz

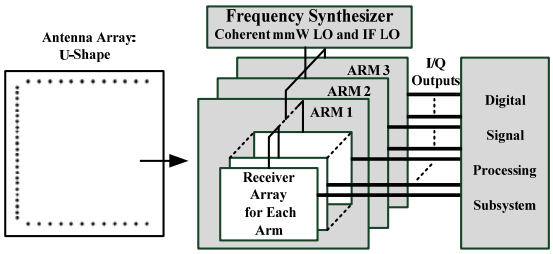

Figure 1. System Configuration of BHU-2D-U

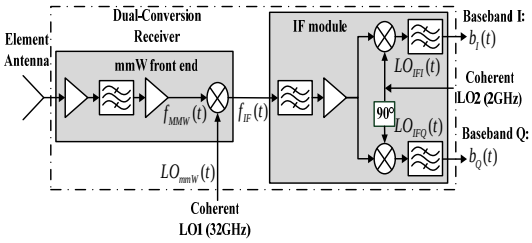

Figure 2. Dual-Conversion Receiver

A 32GHz mmW LO, a 2 GHz IF demodulator LO are required for BHU-2D-U. Figure 2 gives the double side-band dual-conversion receiver block diagram [6]. As Ku and higher frequency multipliers are easy to be integrated in the mmW front-end, 8GHz output is selected for FS. Both LO come from the same reference for coherency. Power divider networks are designed at 2 and 4GHz for lower loss. The preliminary FS design is shown in Figure 3. The analysis on uncorrelated PN effects on Analysis begins with the phase transfer relations inside the dual-conversion receivers, and the factors that affect these requirement settings are found.

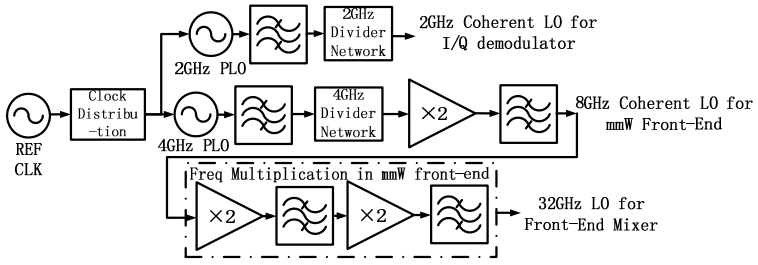

Figure 3. Preliminary FS Design Block Diagram

2.2. Uncorrelated PN Effects Analysis in Visibility Phase Error

Uncorrelated PN is also known as LO phase mismatch between receiver pairs. Firstly, the phase transfer relations inside the receiver chain are concretized. It is assumed firstly that

phase terms of all signals are constant without PN effects. Let $f_{MMW}(t)$, $LO_{mmW}(t)$, $f_{IF}(t)$, $LO_{IFI}(t)$, $LO_{IFQ}(t)$ be the narrow-band mmW received signal and mmW mixer LO, IF down converted signal and IF I/Q demodulator LOs, as shown in Figure 2. They are given as:

$$f_{mmW}(t) = A_{mmW}\cos(\omega_{mmW}t + \emptyset_{mmW}) \quad (1)$$

$$LO_{mmW}(t) = A_{LO1}\cos(\omega_{LO1}t + \emptyset_{LO1}) \quad (2)$$

$$LO_{IFI}(t) = A_{LO2}\cos(\omega_{LO2}t + \emptyset_{LO2}) \quad (3)$$

$$LO_{IFQ}(t) = A_{LO2}\cos(\omega_{LO2}t + \emptyset_{LO2} + 90°) \quad (4)$$

Where $A_{\cdot}$ and $\emptyset_{\cdot}$ are given as the amplitude and phase terms for each signal, and subscripts LO1 and LO2 represent the first and second LO. $f_{IF}(t)$ and $b_i(t)$ are given as:

$$f_{IF}(t) = K_1 f_{mmW}(t) LO_{mmW}(t) \quad (5)$$

$$b_{I,Q}(t) = K_2 f_{IF}(t) LO_{IFI,Q}(t) \quad (6)$$

Where $K_{1,2}$ refers to the conversion loss of the mmW and IF mixer. As the mmW mixer is single side-band and the IF I/Q demodulator is double side-band, the phase terms of $b_I(t)$ and $b_Q(t)$ can be given as:

$$\emptyset_{b_I}(t) = \emptyset_{mmW} - \emptyset_{LO1} \pm \emptyset_{LO2} \quad (7)$$

$$\emptyset_{b_Q}(t) = \emptyset_{mmW} - \emptyset_{LO1} \pm (\emptyset_{LO2} + 90°) \quad (8)$$

From Equation (7) and (8), the phase terms of IF I/Q demodulator output signals are constants. However, PN is always present in a realizable LO, whose phase term can be given by:

$$\emptyset_{LO}(t) = \emptyset_{LO} + \emptyset_n(t) \quad (9)$$

Where $\emptyset_{LO}(t)$ is the phase, $\emptyset_{LO}$ is the definitive phase and $\emptyset_n(t)$ is the time-variant phase drift caused by PN. In SAIR signal processing, the visibility function sample V_{ij} is obtained by cross-correlations between any I/Q output signals calculated in the u-v domain (antenna separation by wavelength), which can be given as [1, 6]:

$$V_{ij} = < b_i(t), b_j(t) > = \frac{1}{\tau_s}\int_0^{\tau_s} b_i(t) \times b_j^*(t)dt \quad (10)$$

Where $b_{i,j}(t)$ is the I/Q output signal (i and j refer to any I/Q demodulated signal, and i can be equal to j), * denotes conjugate signal, and τ_s is the single image integration time (SIIT). Therefore, V_{ij} can be regarded as the integration of the cross-correlations between zero and SIIT time range of BHU-2D-U. Hence it is reasonable to investigate the statistical characteristics of $b_i(t) \times b_j^*(t)$. In SAIR signal processing, visibility phase error is embodied in the expectation of $b_i(t) \times b_j^*(t)$:

$$E[b_i(t) \times b_j^*(t)] = E[A_{b_i(t)} \times A_{bj(t)}^*]E[e^{j(\emptyset_{bi}(t) - \emptyset_{bj}(t))}] = E[A_{b_i(t)}A_{bj(t)}^*]E[e^{j(CPM_{II,IQ}(t))}] \quad (11)$$

Where E[.] is the expectation operator, $A_{b_{i,j}(t)}$ and $\emptyset_{bi}(t)$ are the amplitude and phase of I/Q output signal pairs. A new parameter called Channel Phase Mismatch (CPM) is defined for I-I and I-Q cases in Equation (11) as (same for QQ and QI):

$$CPM_{II}(t) = \Delta\emptyset_{mmW} + \Delta\emptyset_{LO1} \pm \Delta\emptyset_{LO2} \quad (12)$$

$$\mathrm{CPM_{IQ}(t)} = \Delta\emptyset_{\mathrm{mmW}} + \Delta\emptyset_{\mathrm{LO1}} \pm (\Delta\emptyset_{\mathrm{LO2}} - 90°) \quad (13)$$

Where Δ refers to the phase mismatch or uncorrelated PN between channel pairs. It can be observed from Equation (11) and 12 that CPM is the combination of phase mismatches of mmW received signal phase error $\Delta\emptyset_{\mathrm{mmW}}$, mmW mixer LO $\Delta\emptyset_{\mathrm{LO1}}$ and IF IQ LO phase mismatch $\Delta\emptyset_{\mathrm{LO2}}$. $\Delta\emptyset_{\mathrm{mmW}}$ is deterministic and can be calibrated by point source method. $\Delta\emptyset_{\mathrm{LO1}}$ and $\Delta\emptyset_{\mathrm{LO2}}$ could be expanded by Equation (9) as:

$$\Delta\emptyset_{\mathrm{LO1,2}}(\mathrm{t}) = \Delta\emptyset_{\mathrm{LO1,2}} + \Delta\emptyset_{\mathrm{n1,2}}(\mathrm{t}) \quad (14)$$

Where $\Delta\emptyset_{\mathrm{LO1,2}}$ is also deterministic and can be calibrated to zero by point-source method, but $\Delta\emptyset_{\mathrm{n1,2}}(\mathrm{t})$ cannot. It is clear that correlated PN is $\Delta\emptyset_{\mathrm{n}}(\mathrm{t}) = 0$, whereas uncorrelated PN is $\Delta\emptyset_{\mathrm{n}}(\mathrm{t}) \neq 0$. The phase term of Equation (12), which is the visibility phase error, could be simplified by calibration as [1, 6]:

$$\mathrm{E}\left[\mathrm{e}^{\mathrm{j(CPM_{II,IQ}(t))}}\right] = \mathrm{E}\left[\mathrm{e}^{\mathrm{j}(\Delta\emptyset_{\mathrm{mmW}} + \Delta\emptyset_{\mathrm{LO1}} \pm \Delta\emptyset_{\mathrm{LO2}})}\right] \xrightarrow{\text{point source calibration}} \mathrm{E}\left[\mathrm{e}^{\mathrm{j}(\Delta\emptyset_{\mathrm{n1}}(\mathrm{t}) \pm \Delta\emptyset_{\mathrm{n2}}(\mathrm{t}))}\right] \quad (15)$$

Where $\Delta\emptyset_{\mathrm{n1,2}}(\mathrm{t})$ represents the uncorrelated PN in mmW LOs and IF I/Q demodulator LOs, respectively. As in visibility calculation in Equation (10), this phase error of Equation (16) is integrated in time domain and produces imaging errors. From common phase noise theory, a general expression for $\emptyset_{\mathrm{n}}(\mathrm{t})$ in Equation (9) could be further proposed by random phase modulation as [11]:

$$\emptyset_{\mathrm{n}}(\mathrm{t}) = \mathrm{A_n}\cos(\omega_{\mathrm{m}}\mathrm{t} + \psi_{\mathrm{n}}) \quad (16)$$

Where PN is given by random amplitude $\mathrm{A_n}$, offset modulation angular frequency $\omega_{\mathrm{m}} = 2\pi\mathrm{f_m}$ and random phase term ψ_{n}. Therefore, it is observed from the above analysis that $\mathrm{f_m}$ is related to the PN of every LO port, and τ_{s} determines the time range inside which the visibility functions are integrated. Both parameters are significant for uncorrelated PN requirement analysis for SAIR receiver LOs, and a clear relationship between the two should be established for uncorrelated PN control.

3. PN OFR Separation and Requirement Analysis

As PN analysis is mostly performed in frequency domain, a suitable OFR guideline is required to define PN requirements over different OFRs specifically for SAIR imager FS. This separation is different from normal Phase-Locked Oscillator (PLO) phase noise OFR separations, which are known as flicker corner frequency range (FCFR) and in or out of loop bandwidth (ILPBW or OLPBW) frequency ranges. As the 32GHz LO is used in the mmW mixer, it is a more risky LO for uncorrelated phase noise. Hence the requirements on uncorrelated PN are analyzed in detail for the 4GHz and 8GHz FS output ports for visibility phase error control.

3.1. OFR Separation and Uncorrelated Phase Noise Requirements

From Equation (10), the time-domain visibility integration is performed from 0 to τ_{s}, but PN is usually analyzed in the frequency domain. By Fourier Transform, the OFR separation guidelines are given by relations between correlation frequency $\mathrm{f_s} = {}^{1}/_{\tau_{\mathrm{s}}}$ and PN offset frequency $\mathrm{f_m}$. From the perspective of visibility integration phase error control stated in section 2, a PN separation guideline is established for the three OFR separations:

1. $\mathrm{f_m} \gg \mathrm{f_s}$. This range could be interpreted as $\mathrm{f_m} > 100\, f_{\mathrm{s}}$ (Far Offset Frequency Range (FOFR)). This range is far from the actual correlation region, and phase errors caused by uncorrelated PN that lead to visibility errors are negligible.
2. $\mathrm{f_m} < \mathrm{f_s}$ (Very Near Offset Frequency Range (VNOFR)). The correlations of visibility functions actually take place in this region, and uncorrelated PN could cause huge visibility errors. From Equation (15), it is necessary to give limits on phase mismatch and temperature drifts as:

$$\Delta\phi_{\mathrm{OLi}} - \Delta\phi_{\mathrm{OLj}} < 0.5\ deg \quad (17)$$

$$\Delta\phi_{OLi} - \Delta\phi_{OLj} < 0.05\ deg/℃ \quad (18)$$

Where $\Delta\phi_{OLi,j}$ refers to the phase mismatch between different receiver pairs for the same mmW LO. As the phase noise in a certain OFR can be always affected by random fluctuations due to power noise and other reasons, and is highly IC and circuit specific, it is difficult to accurately simulate PN on every offset frequency point. The concept of integrated RMS phase error [12-14] is applied to limit uncorrelated PN. This parameter is previously introduced in the PN control of communication product LOs and ADC clocks [12]. This phase error could be calculated using Figure 4:

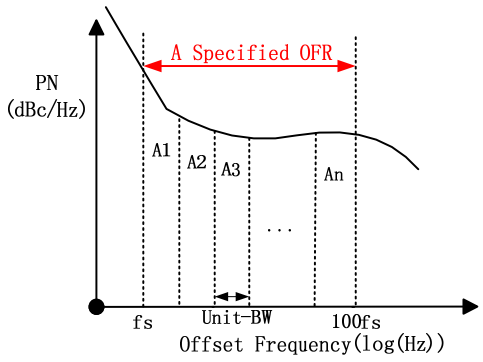

Figure 4. Integrated RMS Phase Error Calculation

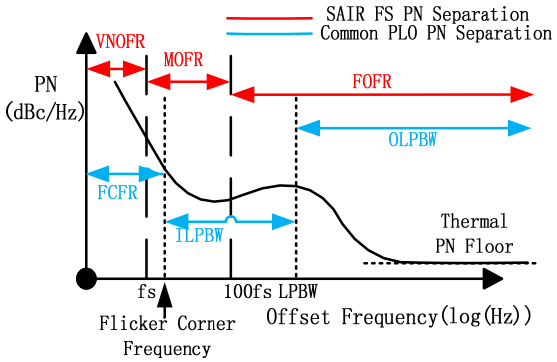

Figure 5. OFR Separation for PN Analysis

The transform from PN to this error is shown in Figure 4. The OFR is divided into N parts in frequency bandwidth, and A_1, $A_2 \ldots A_N$ refer to the integrated phase noise power in dBc in each unit bandwidth (Unit-BW). These Unit-BWs may be unequal due to instrument limitations, and the integrated RMS phase error is calculated as [12-14]:

$$A\ (\mathrm{dBc}) = A_1 + A_2 + \cdots A_N \quad (19)$$

$$\mathrm{PhEr}_{\mathrm{RMS,DSB}}(\mathrm{deg}) = \sqrt{2 \times 10^{A/10}} \times 180/\pi \quad (20)$$

Where $\mathrm{PHEr}_{\mathrm{RMS,DSB}}(\mathrm{deg})$ refers to the integrated RMS phase error, and 2 refers to double side-band (DSB) integration. Therefore, the phase mismatch requirement in Equation (17) can be replaced by:

$$\max\left(\Delta\mathrm{PhEr}_{\mathrm{RMS,4\ GHz,DSB}}(\mathrm{VNOFR})\right) < 0.2\ deg \quad (21)$$

$$\max\left(\Delta\mathrm{PhEr}_{\mathrm{RMS,8\ GHz,DSB}}(\mathrm{VNOFR})\right) < 0.3\ deg \quad (22)$$

Where Δ refer to the difference of integrated RMS phase error between any LO output pairs, so that the maximum delta integrated effect of phase noise mismatch between any 4 and 8GHz output LO signals are defined. These requirements are more stringent than MIRAS (1 deg for phase mismatch and temperature drift), for the working LO frequency (4 and 8GHz) is much higher than MIRAS (1.4GHz) [11].

3. $f_s < f_m < 100\ f_s$. This range is named as Middle Offset Frequency Range (MOFR). The PN variations in this region is easily observed, and they also degrade phase matches by uncorrelated PN between receiver pairs. Therefore, the integrated RMS phase error limit in MOFR can be given as:

$$\mathrm{PhEr}_{\mathrm{RMS,4\ GHz}} = \sqrt{2 \times \int_{f_s}^{100f_s} \mathrm{PN(f)df}} < 1.2\ deg \quad (23)$$

$$\mathrm{PhEr}_{\mathrm{RMS,8\ GHz}} = \sqrt{2 \times \int_{f_s}^{100f_s} \mathrm{PN(f)df}} < 2.4\ deg \quad (24)$$

Where PN(f) is the phase noise measurement results in MOFR, and df is the unit-BW used in the transform. The integrated phase error mismatch could also be defined to limit uncorrelated PN effects in MOFR as:

$$\max(\Delta\mathrm{PhEr}_{\mathrm{RMS,4\ GHz,DSB}}(\mathrm{MOFR})) < 0.1\ deg \quad (25)$$

$$\max\ (\Delta\mathrm{PhEr}_{\mathrm{RMS,8\ GHz,DSB}}(\mathrm{MOFR})) < 0.1\ deg \quad (26)$$

Similarly, the above two limits are set for more stringent control of delta integrated PN effects than MIRAS (1 deg for single side-band 1.4GHz LO) [11].

From the above analysis, the differences between normal PLO OFRs and SAIR FS OFRs are shown in Figure 5. It is clearly demonstrated that these differences and uncorrelated phase requirements are vital for a good SAIR FS design.

3.2. Integration Time Derivation by Temperature Sensitivity

Now τ_s (SIIT) is required to concretize OFR separations for the 4GHz LO. As high imaging rates (HIR) is required by security imaging in BHU-2D-U, video rate imaging with very short SIIT is preferred, but SIIT is limited by the least temperature sensitivity required for effective hazard identification, which is given by [1]:

$$\Delta T \approx \frac{1}{\eta}\frac{T_A+T_R}{\sqrt{B\tau_{st}/2.46}}\frac{\alpha_W}{\alpha_F}\alpha_{LO}\sqrt{N_V} \quad (27)$$

Where η is element antenna efficiency (0.65 of Bode horn); T_A (300K) and T_R (400K) are antenna and receiver noise temperatures; α_W is the window factor (0.53 for hamming window); α_F is the filter factor (1.19 for gauss prediction); N_V is the sampling point number for rectangular visibility function (49×25=1225); B is system bandwidth of 200MHz [15]. The least brightness temperature discrepancy for hazards and human body is 3K, which ΔT must be less than [6]. The total integration time (τ_{st}) is related to the dynamic application condition of security imaging. If a person goes through a 2.5m effective imaging distance with an average walking speed of 1.4m/s, the dwell time is about 1.8s. τ_{st} should be within 1s for 10 images (0.1 s for each image). 0.5 s τ_{st} corresponds to a sensitivity of 2.63K, which leaves some margin from 3K limit. Thus the 0.05 s τ_s (minimum SIIT) is used for OFR separation, with f_s=20Hz, and the three OFRs are f_m<20Hz, 20Hz<f_m<2kHz, f_m>2kHz.

4. Measurement Results and Discussions

4.1. Frequency Synthesizer Design for Uncorrelated PN Requirements

The design of FS PLO must be performed to realize the uncorrelated PN requirements stated above. From conventional PN analysis method in PLO, the VNOFR stays well within the FCFR, and MOFR covers part of FCFR and ILPBW. Therefore, a high frequency (100MHz) and highly stable TCXO is selected as reference. A low PN floor PLO module and a narrow LPBW (40kHz) are designed to realize a lower ILPBW PN for more attenuations on MOFR PN and reference spurs.

4.2. Measurement Results and Discussions

Three output terminals from 4GHz power divider and also from three 8GHz multiplier output ports are selected for PN measurements. The PN profiles and integrated RMS errors are measured by Anritsu MS2692A (Figure 6) for VNOFR, MOFR and FOFR. To decrease the negative effects of random variations of PN over the sweep time, the PN curve of each port is measured consecutively for 10 times and the averaged PN results are shown in Table 2. The PN measurements are performed in single side-band (SSB), whereas integrated RMS phase errors are shown in DSB to realize the requirements. This calculation is done by the instrument automatically using the algorithm in Equation (19) and (20). These results are given in Table 4 and 5, with the unit-BW used is given in Table 3.

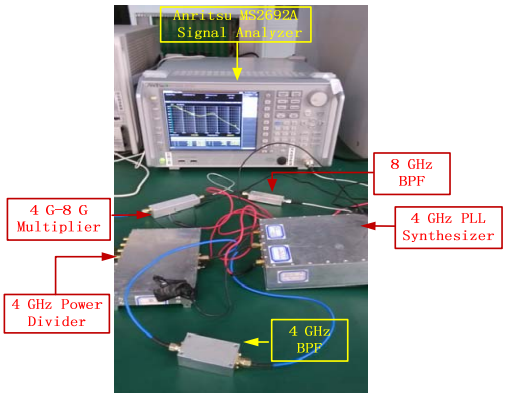

Figure 6. Phase Noise Measurement Setup

Table 2. 4GHz and 8GHz Phase Noise Measurement Results

Offset Freq (Hz)	4 GHz-P1	4 GHz-P2	4 GHz-P2	8 GHz-P1	8 GHz-P2	8 GHz-P3
10	-46.72	-43.65	-43.67	-37.88	-36.83	-37.68
100	-69.79	-67.23	-68.71	-62.08	-65.28	-62.52
1 k	-85.92	-85.70	-86.00	-79.08	-77.68	-79.75
10 k	-93.43	-93.68	-93.10	-86.94	-86.99	-86.90
100 k	-88.61	-88.53	-88.57	-82.22	-82.43	-82.36
1 M	-125.58	-125.68	-125.63	-119.86	-119.84	-119.91
10 M	-139.38	-139.28	-139.02	-140.07	-139.76	-139.91

Table 3. Unit Bandwidth Used in PN to Integrated RMS Phase Error Transform

Offset Frequency Range (Hz)	10~100	100~1 k	1 k~1 M
Unit Bandwidth	1	10	100

Table 4. 4GHz Integrated RMS Phase Error Results (DSB, Deg)

Offset Freq (Hz)	4 GHz-Port1	4 GHz-Port2	4 GHz-Port3	$\max(\Delta \mathrm{PhEr}_{\mathrm{RMS,4\ GHz,DSB}})$
10~20 (VNOFR)	1.472	1.670	1.566	0.198
20~2 k (MOFR)	1.087	1.110	1.079	0.023

Table 5. 8GHz Integrated RMS Phase Error Results (DSB, Deg)

Offset Freq (Hz)	8 GHz-Port1	8 GHz-Port2	8 GHz-Port3	$\max(\Delta \mathrm{PhEr}_{\mathrm{RMS,4\ GHz,DSB}})$
10~20 (VNOFR)	3.197	3.349	3.137	0.212
20~2 k (MOFR)	2.281	2.308	2.287	0.027

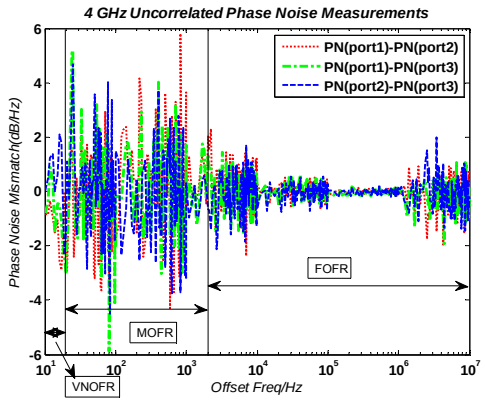

Figure 7. 4GHz Uncorrelated Phase Noise

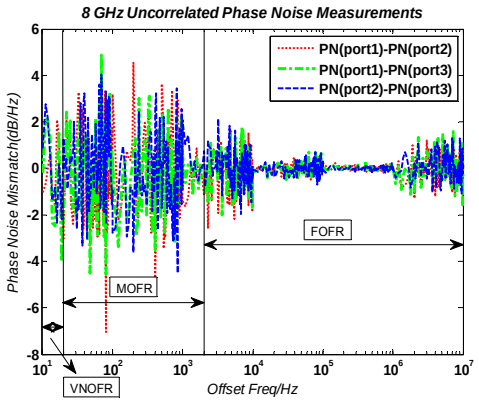

Figure 8. 8GHz Uncorrelated Phase Noise

It is observed from Table 2 that PN mismatch requirements in VNOFR are easily reached, and the maximum delta integrated RMS phase error are well within the limits set by Equation (21) and (22). The more troublesome issue to handle is the temperature drift, for which a fairly stable temperature control system for all receivers must be provided. For MOFR, the integrated RMS phase error of 4GHz and 8GHz LO is limited to 1.2deg and 2.4deg, respectively. The maximum delta phase error of 0.03 deg is realized for both frequencies.

To obtain a clearer picture on uncorrelated phase noise, the phase noise mismatch curves for 4GHz and 8GHz LOs are plotted in Figure 7 and 8. At some offset frequencies in MOFR, this mismatch can reach as high as 6~8dB/Hz. It is observed that in VNOFR and MOFR, the mismatches are much more severe than in FOFR, thus these two figures prove that stringent uncorrelated PN control could never be overlooked in VNOFR and MOFR. The impressions that PN for every offset frequency point and for every output port is the same is only in theory and simulation, and in fact it is not possible to simulate PN on each offset frequency point. The necessity to use integrated RMS phase error to limit the integrated effects of uncorrelated PN on visibility phase errors in SAIR frequency synthesizer design is obviously verified by these measurement results.

5. Conclusion

In this paper, uncorrelated PN effects on visibility errors for BHU-2D-U SAIR system have been investigated in theory and concretized to synthesizer PN mismatch design requirements from phase transfer and system parameter analysis, such as temperature sensitivity. The FS design is given, and the requriements on uncorrelated PN in VNOFR and MOFR are realzied. The existence of uncorrelated PN in VNOFR and MOFR is clearly verified by uncorrelated PN measurement figures. The following findings are clearly observed:

1) Due to HIR imaging requirement of BHU-2D-U required by security imaging, the imaging speed of BHU-2D-U is about 20 frames/s, which is much higher than the MIRAS speed of 3.3 frames/s for earth observation. The OFR separation of BHU-2D-U is thus quite different from MIRAS, as shown in Tab.7. BHU-2D-U MOFR spreads much further into higher offset frequencies than MIRAS, and the bandwidth for uncorrelated PN control is much larger. For this reason, the uncorrelated PN requirements of BHU-2D-U FS is more stringent.

Table 6. MIRAS and BHU-2D-U OFR Comparisons

Parameter	MIRAS	BHU-2D-U
Application	Earth Observation	Security Imaging
Integration Time	1.2 s	0.05 s
Imaging Speed	3.3 Frams/s	20 Frams/s
FOFR	>100 Hz	>2 kHz
VNOFR	<1 Hz	<20 Hz
MOFR	1 Hz~100 Hz	20 Hz~2 kHz

2) Though coherent design and SAIR visibility theory proves that if phase noise is correlated between all LO ports (same PN output at every LO), the LO uncorrelated effects on visibility errors can be neglected, it has been proved by phase transfer analysis and visibility phase error calculation theories that these errors cannot be overlooked in Equation (10) and (15).

A suitable OFR separation is introduced for the SAIR FS to obtain three OFRs: VNOFR, MOFR and FOFR. Stringent uncorrelated PN control is required in VNOFR and MOFR, while FOFR uncorrelated PN can be neglected. The integrated RMS phase error concept used in communication product LOs and ADC clocks is introduced to limit the integrated uncorrelated PN effects in VNOFR and MOFR, and the limits on the mismatch extent of this phase error is also established. By careful FS design, these requirements in VNOFR and MOFR have all been realized.

3) Uncorrelated PN in VNOFR and MOFR is more severe than in FOFR, and this finding has been verified by phase noise measurements in Figure 7 and 8. Uncorrelated PN can be as high as 6~7dB at some offset frequency points in MOFR for the 4 and 8GHz output ports.

This finding has further consolidates the necessity to establish stringent uncorrelated PN control both in VNOFR and MOFR.

The uncorrelated PN requirement analysis proposed by this paper has been designed to fulfill the specific SAIR LO phase noise requirements, and the synthesizer designed has been successfully in operation in BHU-2D-U system. Future optimizations on FS and PN are related to system-level improvement plans.

References

[1] Camps A. Application of interferometric radiometry to earth observation. Ph.D. Dissertation, Polytechnic University of Catalonia, Barcelona, Spain. 1996.

[2] TD Williams, NM Vaidya. *A Compact, Low-Cost, Passive MMW Security Scanner*. Proc. SPIE, 2005; 5789: 109-116.

[3] D Notel, J Huck, S Neubert, S Wirtz, A Tessmann. *A compact mmW imaging radiometer for concealed weapon detection*. Proc. IRMMW-THz, Cardiff. 2007: 269-270.

[4] VG Kolinko, S Lin, A Shek, W Manning, C Martin, M Hall, O Kirsten, J Moore, DA Wikner. *A passive millimeter-wave imaging system for concealed weapons and explosives detection.* Proc. SPIE. 2005, 5781: 85-92.

[5] CA Martin, VG Kolinko. *Concealed weapons detection with an improved passive millimeter-wave imager.* Proc. SPIE. 2004; 5410: 252-259.

[6] C Zheng, X Yao, A Hu, J Miao. A Passive Millimeter-Wave Imager Used for Concealed Weapon Detection. *Progress In Electromagnetic Research B*. 2013; 46: 379-397.

[7] Baohua Yang, Zhiping Li, et.al. Design of Receiver Used for Passive Millimeter Wave Imaging System. *TELKOMNIKA Indonesian Journal of Electrical Engineering*. 2014.

[8] Xianxun Yao, Zhiping Li, et.al. Analysis and Correction of the interchannel mismatch in synthetic aperture radiometer. *TELKOMNIKA Indonesian Journal of Electrical Engineering.* 2013.

[9] Mehdi G, Hu Anyong, Miao Jungang. *Millimetre-wave all symmetric edge-coupled bandpass filter*. The 10th International Symposium on Antennas, Propagation & EM Theory, Xi'an. 2012: 1271-1274.

[10] BH Yang, G Mehdi, AY Hu, et.al. The round ended design and measurement of all symmetric edge-coupled bandpass filter. *Progress in Electromagnetic Research C*. 2013; 38:191-203.

[11] Torres I Corbella, E Castro, et.al. *Phase noise requirements in interferometric radiometers*. IGASS. 2009; 3: 1027-1030.

[12] Brannon B. *Sampled systems and the effects of clock phase noise and jitter*. Analog Devices Inc, Report Number: AN-756.

[13] Shinagawa. M, Jitter analysis of high-speed sampling systems. *IEEE Journal of Solid-state Circuits*, 1990, 25(1): 220-224.

[14] W Kester. *Converting oscillator phase noise to time jitter*, Analog Devices Inc, Report Number: MT-008.

[15] C Zheng, X Yao, A Hu, et.al. Closed form calibration of 1bit/2level correlator used for synthetic aperture interferometric radiometer. *Progress In Electromagnetic Research M*. 2013; 29: 193-205.